IEEE Access
Multidisciplinary | Rapid Review | Open Access Journal

Received January 16, 2019, accepted January 27, 2019, date of publication February 18, 2019, date of current version March 1, 2019.

Digital Object Identifier 10.1109/ACCESS.2019.2898091

Frequency Difference EIT With Localization: A Potential Medical Imaging Tool During Cancer Treatment

CHENNING WU AND MANUCHEHR SOLEIMANI
Engineering Tomography Laboratory, Department of Electrical and Electronic Engineering, University of Bath, Bath BA2 7AY, U.K.
Corresponding author: Chenning Wu (cnw24@bath.ac.uk)

ABSTRACT Electrical impedance tomography (EIT) has attracted great interest in a number of medical applications. It offers several unique advantages, such as being safe, low cost, and having high temporal resolution over other tomographic imaging protocols. The frequency dependence of electrical conductivity in biological samples gives EIT imaging a renewed chance to be a monitoring technique for new and very important medical applications, such as tumor tracking during radiation therapy. Therefore, frequency difference EIT (fdEIT), which reconstructs images using difference data at two injecting frequencies, is a good candidate for high-speed tissue characterization in dynamical settings. However, a low spatial resolution of EIT is a major drawback that limits its uses. In some cases, such as the treatment of tumors, prior knowledge about the location of a tumor is provided by early diagnostic images. This prior knowledge coupled with the spectroscopic knowledge of the frequency response of a tumor against normal tissue gives a possibility for localized fdEIT imaging, which can significantly enhance the spatial resolution. The experimental results in this paper demonstrate this for the purpose of such monitoring of an inclusion exhibiting frequency-dependent impedance and are quantitatively compared with traditional methods. The new method's performances and robustness are demonstrated numerically using several image quality measures. This could give the EIT new roles to play, for motion compensation in conjunction with the traditional low-speed but high-resolution medical imaging systems and dynamic tumor tracking.

INDEX TERMS EIT for tumor tracking, weighted frequency difference, total variation, region of interest, image evaluation parameter.

I. INTRODUCTION

Medical imaging for cancer diagnosis requires high resolution imaging systems such as Magnetic Resonance Imaging (MRI) and X-ray computed tomography (CT). However, these high resolution imaging systems can only provide accurate but static assessment due to their inherent low data capture rate; this may be insufficient during cancer treatment, for instance in radiotherapy, in which respiration-induced tumor motion information is required for accurate targeting. There are various approaches to detect and estimate the respiratory movement, such as surrogate devices for the detection of the chest wall movement and metallic seeds implanted into a patient's body [1]. Yet none of them manage to achieve an accurate tracking of tumor movement with patient friendly operations.

Electrical Impedance Tomography (EIT) is an imaging modality that injects electrical currents to the electrodes attached to the periphery of the electrically conductive objects and takes electrical measurements from the remaining electrodes to image the impedance distribution within the medium. EIT was introduced as a safe, rapid, non-invasive, and non-cumbersome way of visualizing electrical properties of human body tissues, especially large organs, by Barber and Brown [2]. As EIT virtually causes no adverse side effects (lack of radiation, no transport required), the method has become an attractive alternative to CT, MRI or ultrasound examinations. The key advantage of EIT is its relatively high acquisition speed, which can reach up to a few hundreds of frames/s in modern EIT devices as opposed to approx. 150 ms/frame in CT and even a few

The associate editor coordinating the review of this manuscript and approving it for publication was Zhaoqing Pan.

minutes per frame in PET [3]. Consequently, it provides the availability of powerful temporal filtering techniques, which means that it can detect the dynamic behavior of tissues; and hence, it can provide unique clinical information difficult to obtain by other technologies at bedside. Such algorithms allow EIT to be developed in thoracic functional applications, such as monitoring of mechanical ventilation, monitoring of heart activity and lung perfusion, and pulmonary function testing [4]. As a result, EIT can be introduced as a guidance during a treatment session, though it may not be available of the same level as in the diagnostic stage. Studies on combining EIT with other slow but high spatial resolution imaging systems, cone beam computed tomography (CBCT) for example, have been done [1], [5], [6]. In these works, EIT is employed to exact and provide lung motion information to CBCT for motion compensation so that more accurate tumor imaging can be achieved for image-guided radiation therapy.

In this paper, EIT is presented as a direct tumor tracking tool in cancer treatment application. The prior diagnostic knowledge provides the area within which the tumor is moving so that the reconstruction can be restricted to a region of interest (ROI). By applying such localized reconstruction techniques, the sensitivity within the ROI can be refined and the image resolution can therefore be enhanced [7]–[9]. Successes of introducing localized reconstruction strategies to improve image quality have been obtained both in industrial and medical areas, such as multi-phase pipeline flow analysis [10], assessment of regional lung ventilation [11]–[13] and potentially vocal folds monitoring [7]. Additionally, in the tumor tracking practice, baseline data is mostly unavailable. Therefore, frequency difference EIT (fdEIT) reconstruction that recovers the changes in impedance with respect to stimulation frequencies instead of time (tdEIT) will be implemented. This is based on the frequency dependent impedance of bio-samples and the development of multi-frequency EIT with a high data acquisition speed brings feasibility of fdEIT to clinical tracking applications [14].

The idea of monitoring tumor movement using fdEIT within the localized region was brought up in [15], however, it was only demonstrated with simulation results and was lacking experimental evidence. In this work, following the success of simulation results presented in [15], two-dimensional phantom experiments using bio-samples were implemented to study the feasibility of the proposed technique Specially, objects were placed at horizontally varying locations within a central limited region to simulate tumor movement in the anterior-posterior (AP) direction. Reconstructions were conducted by using the Total Variation (TV) functional [16], [17] to overcome the over-smoothed effect brought by traditional Tikhonov regularization. Results will be compared with traditional global reconstruction as well as mathematically modified global reconstruction to further validate and verify the proposed methodology; and hence offer the confidence in further in vitro or in vivo body tissue experiments.

II. ELECTRICAL IMPEDANCE TOMOGRAPHY

A. FORWARD PROBLEM

EIT is the process of constructing a conductivity distribution from sets of voltage measurements when stimulated with current from different combinations of electrodes. Before image reconstruction, some pre-calculations and modeling of how a change of conductivity within the view region will affect the boundary measurements, which is referred to as the forward problem, are conducted. To model the relationship between electric potential from the electrodes and the conductivity within the body, the derivation of Maxwell's equation can be introduced as below:

$$\nabla \cdot (\sigma \nabla u) = 0 \tag{1}$$

where σ is the conductivity, u is the electric potential distribution, and $\nabla\cdot$ is the divergence operator. In the forward problem, the voltage is predicted from any given current density within the field under the assumption of a constant conductivity. To solve the forward problem, the finite element method (FEM) has been used.

B. INVERSE PROBLEM

EIT reconstruction is the process of estimating conductivity from the boundary voltage measurements $\boldsymbol{V_{meas}}$, which is also known as the inverse problem,

$$\boldsymbol{V_{meas}} = \boldsymbol{F}(\boldsymbol{\sigma}) + \boldsymbol{e} \tag{2}$$

where $\boldsymbol{F}$ is a forward operator, which estimates the boundary voltages using linear approximation from calculated Jacobian, and $\boldsymbol{e}$ is the mismatch between measurements and the estimation from the forward model. In EIT, it is common to simplify (2) by using a linear approximation:

$$V_{meas} - \boldsymbol{F}(\sigma_0) \approx J(\sigma - \sigma_0) \tag{3}$$

where J is the Jacobian or sensitivity matrix of $\boldsymbol{F}$ calculated at the initial conductivity estimate σ_0. Defining $\Delta\sigma = \sigma - \sigma_0$, and $\Delta V_{meas} = V_{meas} - \boldsymbol{F}(\sigma_0)$, then (3) can be written as:

$$\Delta V_{meas} = J\Delta\sigma. \tag{4}$$

The conventional method of solving (4) is seeking to minimize the residual:

$$argmin\left(\|\Delta V_{meas} - J\Delta\sigma\|^2\right). \tag{5}$$

In inverse problems, the imaging process may result in a loss of information due to the noisy and discretely sampled data. Hence, EIT reconstruction is considered as ill-posed in that simply finding the least square solution is unable to overcome the instability of the solution. Rather, regularization needs to be applied to smooth ill-posed problems by either truncating small values in the sensitivity matrix or imposing additional information about the solution:

$$\Delta\sigma = argmin\left(\frac{1}{2}||\Delta V_{meas} - J\Delta||^2 + \alpha R(\Delta\sigma)\right) \tag{6}$$

where α is the regularization parameter controlling trade-off between regularization and fidelity; and R is the regularization functional.

The standard L^2- norm regularization algorithm, e.g. the most widely used one Tikhonov regularization method, can be formulated as below:

$$\Delta\sigma = argmin(\|\Delta V_{meas} - J\Delta\sigma\|^2 + \alpha L\,\|\Delta\sigma\|^2) \quad (7)$$

where L, the regularization matrix, is commonly an identity matrix or diagonal matrix. The standard Tikhonov method is realized by replacing L with the identity matrix [18], then (7) can be formulated as:

$$\Delta\sigma = (J^T J + \alpha I)^{-1} J^T \Delta V_{meas}. \quad (8)$$

The penalty term in L^2-norm regularization penalizes a large gradient of the conductivity and yields smooth reconstructions. As a result, they won't preserve a sharp object boundary, and hence are not highly regarded in the medical applications.

The total variation regularization, on the other hand, adopts the L^1 norm which doesn't penalize image discontinuities and helps to preserve the boundaries of perturbations and sharp changes in conductivity. This is particularly attractive for reconstructing sharp transitions [16], [19] as it would improve the characterization of the object's size and shape.

III. METHODOLOGY

A. FREQUENCY DIFFERENCE EIT

EIT reconstruction is mainly categorized into two types, difference imaging and static imaging. Static imaging attempts to recover images of the absolute impedance distribution of the medium, which only requires one set of measurements at one instance. Nevertheless, it has suffered from a limited amount of measurable information, unknown boundary geometry, uncertainties in electrode positions. Difference imaging, on the other hand, recovers an estimate of the change in impedance, and hence greatly overcomes the drawbacks of absolute EIT by cancelling out common errors through data subtraction to allow reconstructions to remain stable. One approach is to adopt a time-difference (tdEIT) imaging method, where the change of impedance in sensing area between two instances is reconstructed. However, in the cases of tumor imaging or stroke detection when time-referenced data is not available, tdEIT method is not applicable [20], [21]. Given the fact that biological tissues have different frequency responses [22]–[24], impedance distribution inside the viewing region can be imaged by frequency difference reconstruction method (fdEIT), where measurements are taken under at least two frequencies.

However, a simple frequency difference may not completely benefit from the advantages provided by difference imaging as various errors may occur at different frequencies. Consequently, weighted fdEIT reconstruction was proposed and has been validated by numerical simulations and phantom experiments [20], [25]–[27]. It is particularly useful in medical applications where the background is always composed of other body tissues that also have frequency dependent characteristics, and then the background influence can be eliminated while maintaining the impedance contrast within the anomaly. Then the boundary voltage measurement ΔV_{meas} is denoted as:

$$\Delta V_{meas} = V_{f_2} - aV_{f_1} a = \frac{\langle V_{f1}, V_{f2}\rangle}{\langle V_{f1}, V_{f1}\rangle} \quad (9)$$

where $\boldsymbol{V_{f_1}}$ and $\boldsymbol{V_{f_2}}$ are the measurements collected at frequencies $\boldsymbol{f_1}$ and $\boldsymbol{f_2}$ respectively; $\boldsymbol{a}$ is a frequency weight factor and $\langle\cdot,\cdot\rangle$ is the standard inner product of two vectors.

In the medical applications, a set of stimulation frequencies will be carefully selected so that the frequency contrast of the anomalies is distinguishable from that of the background.

B. TOTAL VARIATION REGULARIZATION BASED ON SPLIT BREGMAN FORMULATION

The total variation problem is defined by replacing the penalty term L1 norm of the gradient of the image:

$$R(\Delta\sigma) = \|\nabla\Delta\sigma\|_1 \quad (10)$$

where $\|\cdot\|_1$ denotes the L1 norm, and ∇ is the gradient.

The unconstrained formulation for the linearized model of EIT problem as following:

$$\Delta\sigma = argmin\left(\frac{1}{2}\|J\Delta\sigma - \Delta V_{meas}\|_2^2 + \alpha\,\|\nabla\Delta\sigma\|_1\right). \quad (11)$$

The introduction of the TV method, however, makes the inverse problem non-differentiable, so the traditional gradient class inversion algorithms are not applicable.

In this paper, minimization of functions of TV norms is solved by the Bregman iteration technique, i.e. error forgetting [28], which benefits the advantages of quick convergence and a constant regularization parameter. The split Bregman algorithm, that combines the Bregman distance with splitting technique, was proposed in [29]. It was proved a good performance when applied to EIT with higher resolution, better noise resistivity and faster convergence compared with other TV algorithms [17], such as linearized alternating direction method of multipliers (LADMM). This makes SB TV algorithm a good candidate especially in medical applications.

The implementation of the split Bregman method can be accomplished by introducing auxiliary variables to separate the non-differentiable L^1-norm penalty term and L^2-norm functional so that they can be solved in two alternating steps. Then (11) becomes a constrained optimization problem:

$$\Delta\sigma = argmin(\frac{1}{2}\|J\Delta\sigma - \Delta V_{meas}\|_2^2 + \alpha\,\|d\|_1) \quad s.t.\ d = \nabla\Delta\sigma \quad (12)$$

where d is an auxiliary variable.

The corresponding unconstrained solution of (12) by applying the Lagrange equation is

$$\Delta\sigma = argmin\frac{1}{2}\left\|J\Delta\sigma - \Delta V_{meas}\right\|_2^2 + \alpha\left\|d\right\|_1 + \frac{\beta}{2}\left\|d - \nabla\Delta\sigma\right\|_2^2 \quad (13)$$

where β is the split parameter.

Applying the Bregman iteration method, the original problem can be transformed into the following sub-problems:

$$\left(\Delta\sigma^{k+1}, d^{k+1}\right) = argmin\frac{1}{2}\left\|J\Delta\sigma - \Delta V_{meas}^k\right\|_2^2 + \alpha\left\|d\right\|_1 + \frac{\beta}{2}\left\|d - \nabla\Delta\sigma - b_d^k\right\|_2^2 \quad (14)$$

$$b_d^{k+1} = b_d^k + \nabla\Delta\sigma^{k+1} - d^{k+1}. \quad (15)$$

The minimization of (14) can be handled by separately solving the minimization of $\Delta\sigma$ and d as below:

$$\Delta\sigma^{k+1} = argmin_{\Delta\sigma}\left(\frac{1}{2}\left\|J\Delta\sigma - \Delta V_{meas}^k\right\|_2^2 + \frac{\beta}{2}\left\|d - \nabla\Delta\sigma - b_d^k\right\|_2^2\right)$$

$$d^{k+1} = argmin_d\left(\alpha\left\|d\right\|_1 + \frac{\beta}{2}\left\|d - \nabla\Delta\sigma^{k+1} - b_d^k\right\|_2^2\right).$$

This was computed as the following procedure and initially assign value to $\Delta\sigma^0 = 0$, and then set $d^0 = b_d^0 = 0$:

Step 1: $B\Delta\sigma^{k+1} = \beta\left(d^k - b_d^k\right) + J^T\Delta V_{meas}^k$,
where $B = J^TJ + \beta I$

Step 2: $d^{k+1} = shrink(\Delta\sigma^{k+1} + b_d^k, {}^{\alpha}/_{\beta})$

Step 3: $b_d^{k+1} = b_d^k + \Delta\sigma^{k+1} - d^{k+1}$

Step 4: $\Delta V_{meas}^{k+1} = \Delta V_{meas}^k - J\Delta\sigma^{k+1}$

In addition to the Total Variation regularization discussed above, a Bescov regularizer was proposed and evaluated to produce a superior image reconstruction [29], that is, the regularization term becomes $\|u\|_{BV} + \|u\|_{B1,1}$. The inclusion of multiple regularizers helps to reconstruct smooth images with little effect on the convergence time.

C. LOCALIZED RECONSTRUCTION

The conventional algorithm reconstructs images over the entire medium without emphasis on the information in the region of interest. The main drawback of the traditional algorithm is that the ill-posedness nature of EIT inherently results in a high sensitivity to the changes occurring near the boundary than those in the middle of the medium [30]. This will impose a more significant effect when the targets to be recovered are rather small and the changes in impedance caused by objects could severely be contaminated by noise occurring at the boundary. A strategy using all boundary measurements to reconstruct images within a defined ROI is proposed in this paper to enhance image resolution. Applying ROI is equivalent to the conventional reconstruction but with more independent measurements. Since Jacobian is non-uniform and ROI is normally defined to be far away from the boundaries, chances are noises occurring near the boundaries might not be picked up by ROI or not have the same effect as they are to the global reconstructions. In the content of our proposed applications, i.e. tumor monitoring, the location of the tumor can be initially determined by traditional CT scan and will be utilized as prior knowledge in the EIT reconstruction. Subsequently, a sub-volume in this case can be selected larger than the size of the tumor to allow for the respiration-induced tumor movement.

The conventional global reconstruction can be formulated as (15) considering that the sensing field is discretized into N_F elements and there are N_M independent measurements.

$$[J]_{N_M\times N_F}[\Delta\sigma]_{N_F\times 1} = [\Delta V]_{N_M\times 1}. \quad (16)$$

The principle of ROI reconstruction is restricting the image reconstruction process to a sufficiently large ROI that covers the anomaly completely. Therefore, the original medium can be divided into two areas: one is the conductivity-varying area, which is known as ROI; the other is constant-conductivity area that $\Delta\sigma$ is zero. Assuming the ROI consists of N_{ROI} elements and the remaining elements N_P correspond to the zero conductivity change. Now the conductivity vector becomes

$$[\Delta\sigma]_{N_F\times 1} = \left[\Delta\sigma_1, \cdots, \Delta\sigma_{N_{ROI}}, 0, \cdots, 0\right]^T \quad (17)$$

and yields the reconstruction equation:

$$\left[J_{N_M\times N_{ROI}} J_{N_M\times N_P}\right]\begin{bmatrix}\Delta\sigma_{N_{ROI}\times 1}\\ 0_{N_P\times 1}\end{bmatrix} = [\Delta V]_{N_M\times 1}. \quad (18)$$

Equation (17) can then be reduced to:

$$[J]_{N_M\times N_{ROI}}[\Delta\sigma]_{N_{ROI}\times 1} = [\Delta V]_{N_M\times 1}. \quad (19)$$

Therefore, the way of achieving the localized reconstruction is to restrict the Jacobian matrix to that in (11). The improvement of imaging can be interpreted by considering Jacobian matrix, which represent the sensitivity of the measurements at the boundary to the changes occurred inside the medium. By properly resizing the Jacobian matrix, the sensitivity to the changes happening outside the ROI can be weakened. This can bring several advantages:

1) The elements with constant conductivity are no longer included in the reconstruction process; therefore, the chances of accumulating zero-conductivity change can be reduced;
2) The condition for (11) to have unique solution is now $N_{ROI} < N_M$ rather than $N_P < N_M$;

IV. EXPERIMENTS

Feasibility studies of the proposed method were carried out experimentally. In this paper, only 2-dimensional models were considered.

TABLE 1. Theoretical model and reconstructions of large sample.

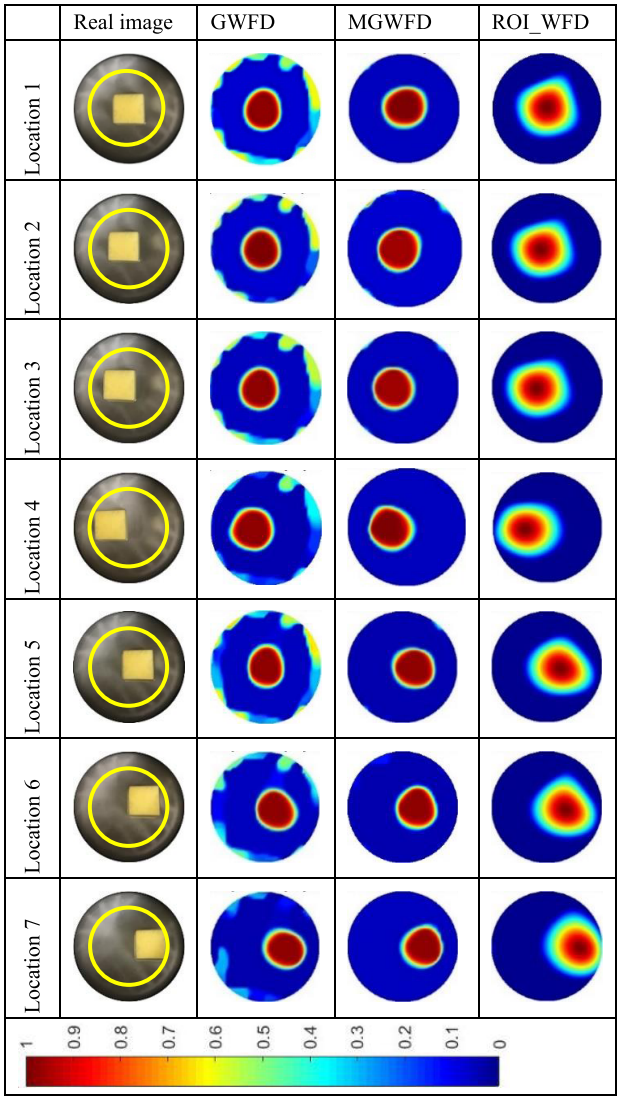

TABLE 2. Theoretical model and reconstructions of medium sample.

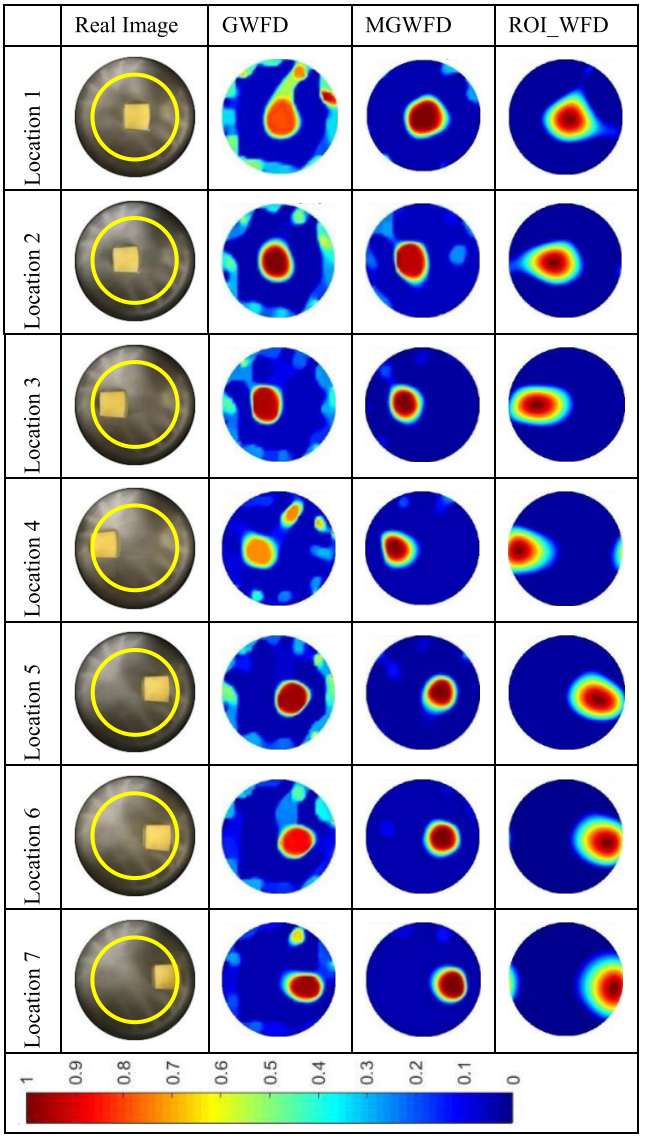

A. MEASUREMENT SYSTEM SETUP

Phantom experiments were established in a cylindrical tank of 19 cm diameter, with 16 equally spaced stainless-steel electrodes on the periphery. EIT measurements were carried out with a 16 channel KHU Mark 2.5 EIT system, which injects 2 mA currents over a wide range of frequencies from 10 Hz to 500 kHz. An adjacent injection method was implemented that results in a total of 208 measurements per frame. To improve the precision of reconstruction, measurements are typically averaged over many data frames, and in the experiments presented, measurements at each location are results of averaging over 20 frames.

Three sets of experimental tests were considered. In all cases, four realizations of EIT measurements were collected: V_{f1} and V_{b1} corresponding to measurements of background only and with inclusion under 1 kHz stimulation respectively; and V_{f2} and V_{b2} corresponding to measurements of background only and with inclusion under 50 kHz stimulation respectively. Potato pieces were chosen to simulate tumor tissue and were placed in 0.5% saline water (conductive background). Objects to be reconstructed are in the sizes of 3.5 cm $\times$ 3.5 cm, 2.5 cm $\times$ 2.5 cm and 2 cm $\times$ 2 cm, and each is placed at horizontally various locations within a pre-defined area (bold yellow circle in Table 1, table 2 and Table 3) in the phantom.

B. EXPERIMENT PROCEDURE

In each of the three cases, reconstructions can be computed in three different protocols:

- Conventional global weighted frequency difference (GWFD) reconstruction as formulated in equation (6).
- Modified global weighted frequency difference (MGWFD) reconstruction, which subtracts common

TABLE 3. Theoretical model and reconstructions of Small sample.

	Real image	GWFD	MGWFD	ROI_WFD
Location 1	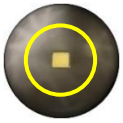	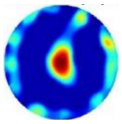	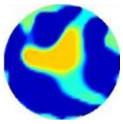	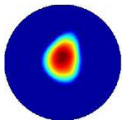
Location 2		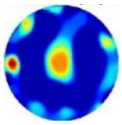	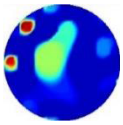	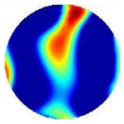
Location 3		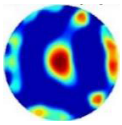	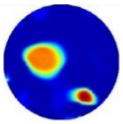	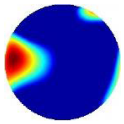
Location 4		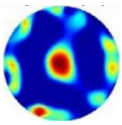	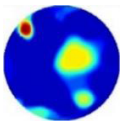	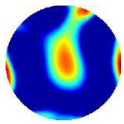

errors in the background from the measurements

$$\Delta V_{data} = (v_{f_2} - \alpha v_{f_1}) - (v_{b_2} - \beta v_{b_1}),$$
$$\beta = \frac{\langle V_{b1}, V_{b2} \rangle}{\langle V_{b1}, V_{b1} \rangle}.$$

- Limited region weighted frequency difference (ROI_WFD) reconstruction. The region of interest is defined by applying a threshold of 0.6 over the entire view region.

As suggested above, in addition to the conventional global reconstruction, a modified global reconstruction that subtracts the common background noise from the original datasets was also performed to compare with the proposed method. Considering the tumor tracking application, where background data is no longer available, MGWFD reconstruction is only accessible in the lab scenario for verifying the significance of the proposed technique.

Image reconstructions were performed by solving the forward problem using EIDORS (Electrical Impedance and Diffuse Optical tomography Reconstruction Software), which is a software suite implemented in MATLAB, and implementing Split Bregman Total Variation regularization to solve inverse problem. The resulting impedance distribution is normalized since only the size and location of the objects are considered.

C. RESULTS

In this section, reconstructed images of three samples using the proposed method, i.e. ROI_WFD, as well as the conventional algorithm with and without data modification are presented. All three sets of results are compared with real images. When applying ROI_WFD, the entire reconstruction region is limited to the ROI as previously defined and is compared with the view region within the yellow solid circle in each real image.

In Table 1, all three columns of reconstructed images manage to recover the real images. Yet, it is still worth noting that both MGWFD and ROI_WFD are able to remove the noise effect presented in GWFD.

In table 2, a series of medium objects were tested and image reconstruction results are presented. When compared with the large sample case, a consistency of error existence in the left-top of the tank is seen in the GWFD reconstructed images. Again, a better image quality (in terms of getting rid of the background artifacts) was achieved by both MGWFD and ROI_WFD.

The small object case unsurprisingly gives the worst image reconstructions as shown in Table 3. With the presence of noise, the signal is more prone to be contaminated. Moreover, facts that potato samples can absorb from background saline water by osmosis, the conductivity of potato samples can change as the experiments went along. Therefore, using the GWFD failed to track the movement of object. Even with a modified dataset, the inherent ill-posed nature of EIT still gives rise to difficulties on reconstructing images without the disturbance of the noise signal. Reconstruction using ROI_WFD also experiences a notable image distortion, but still shows a better location matching in comparison with GWFD. Further quantitative image quality analysis is required to justify the significance of ROI_WFD in the next section.

V. ANALYSIS AND DISCUSSIONS

To further compare the results of the proposed methods with the other two, three evaluation parameters are used in this section. Position error (PE) and resolution (RES), which are selected based on [31], together with relative error (RE) of each reconstruction are plotted against different locations to evaluate images. Each image is comprised of 200×200 pixels and can be represented by a column vector $\hat{x}$. A threshold of one-fourth of the maximum amplitude is applied, which detects most of the visually significant effects:

$$[\hat{x}_q]_i = \begin{cases} 1, & \& \, [\hat{x}_q]_i \geq \frac{1}{4}\max\hat{x}) \\ 0, & otherwise. \end{cases} \tag{20}$$

A. POSITION ERROR

Position error describes the difference between the center of mass of the real P_0 and reconstructed images P_q,

$$PE = \left| P_0 - P_q \right|. \tag{21}$$

PE is preferably as small as possible so that the it can provide reliable results in locating the tumor; hence PE is of the most importance figure of merit in our case so that the confidence in tumor tracking applications can be assured.

Figure 1 to Figure 3 plot the position error of three samples in centimeters against location variation.

The position error plot of the large object does not suggest a notable improvement using the proposed method in

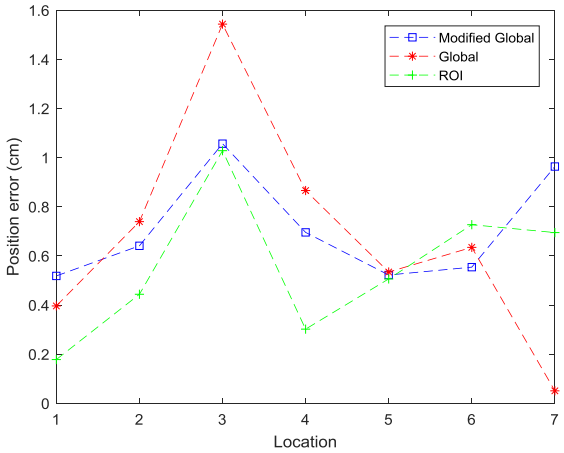

FIGURE 1. Position error plots of large object.

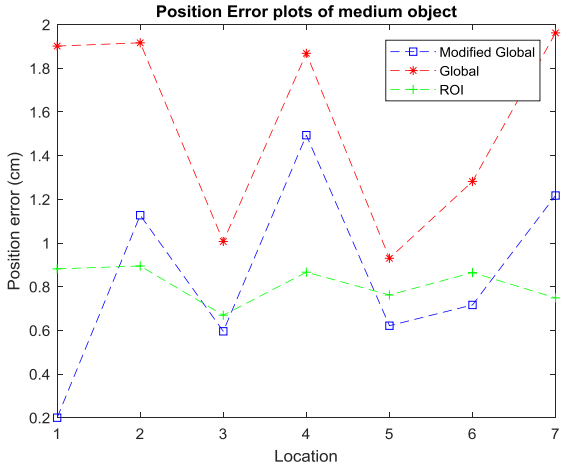

FIGURE 2. Position error plots of medium object.

comparison with the conventional method using both the modified and original datasets. This is due to the sufficient impedance contrast in large sample tests compared to the background noise that has been introduced. Yet, as the size of the inclusion decreases, position errors tend to increase massively with all three protocols. However, using ROI_WFD not only provides comparable results to a de-noised dataset, but also shows a better consistency of position displacements. This is advantageous as it provides the possibility of data calibration in practice.

B. RESOLUTION

Resolution measures the size of reconstructed inclusion as a fraction of size of entire imaging region. In this paper, it is defined as the area ratio of the recognizable anomaly to the entire sensing area instead of the diameter ratio as suggested in [31]:

$$RES = \sqrt{A_q}/A_0 \tag{22}$$

where $A_q = \sum_k \left[\hat{x}_q\right]_k$ is the number of pixels in $\hat{x}_q$ and A_0 is the number of pixels over the entire medium region. RES should be uniform and small, in order to accurately represent the shape of the target conductivity distribution.

Resolution plots of three objects at different locations are presented above in Figure 4, Figure 5, and Figure 6. Theoretical resolutions calculated from the real image are also plotted in each figure as a reference. Evidently, reconstructions using ROI_WFD perform the best in terms of preserving the uniform resolution. Similar to position error plots, the advantages of using the proposed method become more significant as the object size gets smaller. Interestingly, ROI_WFD is even seen a degradation of matching with the theoretical RES, which suggests that it will be particularly useful when the tumor size is at least smaller than 13% of the view region.

C. RELATIVE ERROR

Relative error, which quantifies the difference between the reconstructed image and the real image with respect to the

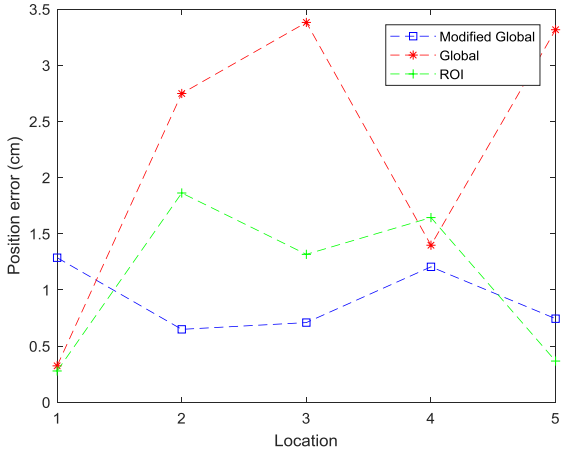

FIGURE 3. Position error plots of small object.

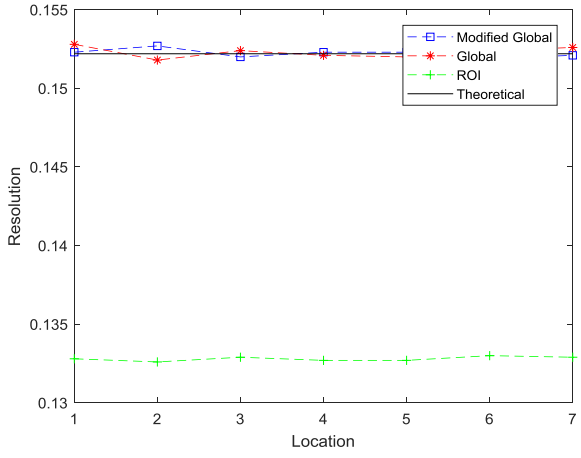

FIGURE 4. Resolution plots of large object.

real image, can be defined as:

$$RE = \frac{\left\|x_0 - \hat{x}_q\right\|_2}{\|x_0\|_2} \tag{23}$$

where x_0 is the pixel vector of the real image. As the definition suggests, the smaller RE is, the higher quality of the

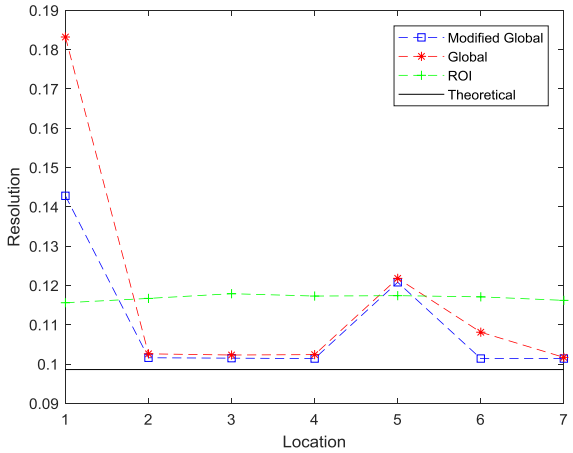

FIGURE 5. Resolution plots of medium object.

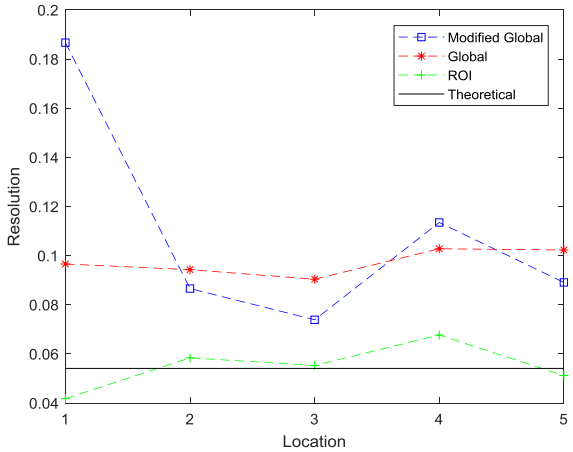

FIGURE 6. Resolution plots of small object.

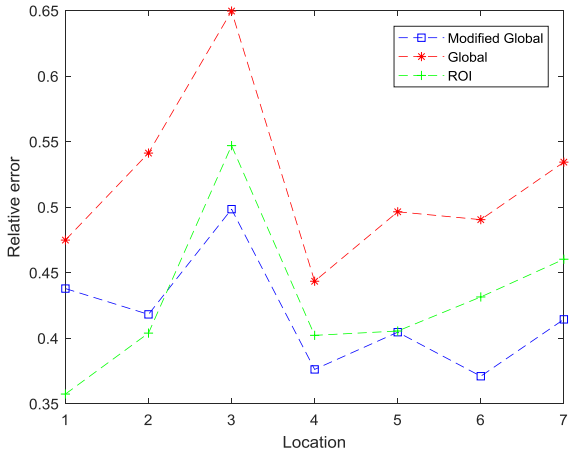

FIGURE 7. Relative error plots of large object.

reconstructed image it is. Figure 7, Figure 8 and Figure 9 plotted relative errors of large, medium and small objects against locations respectively

An overall increase of relative error is suggested with the size of the inclusions decreasing. As a smaller object will yield a smaller impedance change and hence a weaker

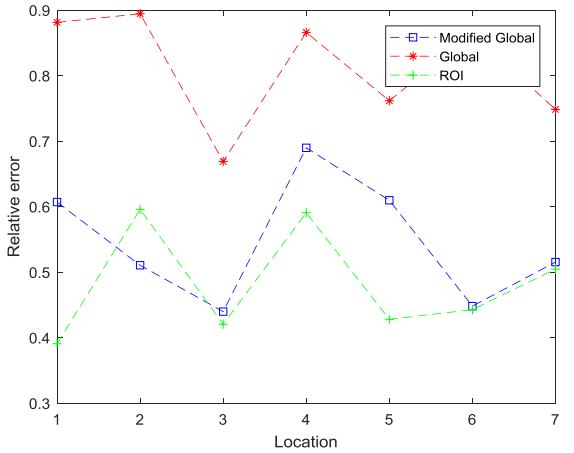

FIGURE 8. Relative error plots of medium object.

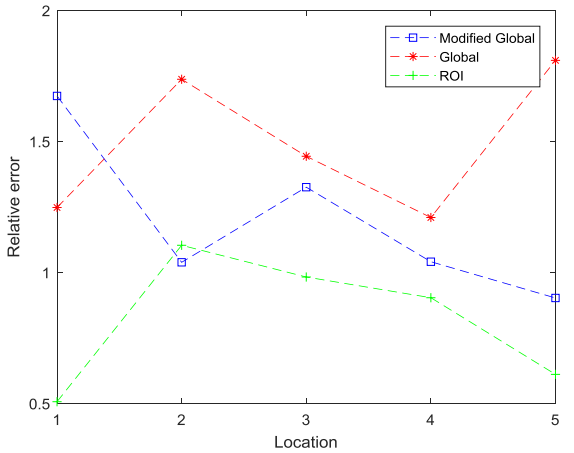

FIGURE 9. Relative error plots of Small object.

sensing signal, assuming the same amount of noise presented in the system, it will be more difficult to extract the information from the background noise. Among the three methods, ROI_WFD provides the best RE results in small inclusion tests and minimizes the background error to the similar extent as using the modified datasets, MGWFD.

VI. CONCLUSION

Tumor treatment using radiation therapy often requires a conventional imaging system, such as volumetric X-ray CT and PET prior to a treatment session. The organ movement can be a major source of artifacts in these imaging systems with low temporal resolution. In this work, a weighted frequency difference reconstruction within the region of interest is proposed and validated by two dimensional phantom experiments. This method offers EIT an opportunity of being considered as a tracking tool in tumor treatment applications.

To simulate the proposed application, bio-samples of different sizes were selected and placed at various locations within a pre-defined fraction of area in the phantom. Images were reconstructed using Split Bregman Total Variation regularization and the image quality was analyzed by using

position error, resolution and relative error. An improvement can then be confirmed by comparing the results from ROI_WDF to conventional GWFD as well as MGWFD, especially in the cases of tracking small samples. Moreover, the proposed method applies a filtering effect of noise as the results are comparable with MGWFD. This is particularly useful in the tumor tracking cases, where the background noises caused by contact impedance between electrodes and skin as well as other organs' movements are significant. These noises cannot be removed by MGWFD in practice due to the lack of background data whereas the proposed method, ROI_WDF, achieves the similar noises subtraction effect, and hence can be introduced into such applications.

With the confidence obtained from both 2-D simulation and experiment results, this limited region based EIT with frequency difference imaging could potentially be considered as a key tool for treatment planning and treatment monitoring. Further 3-D experiments would be beneficial as in such cases capturing tumor motion would be more challenging. The proposed localized EIT system will create potential for motion compensation data for PET and CT. Additionally the proposed method here can extend to tracking tumors during radiation therapy making an adaptive radiation therapy possible.

REFERENCES

[1] T. Pengpan, N. D. Smith, W. Qiu, A. Yao, C. N. Mitchell, and M. Soleimani, "A motion-compensated cone-beam CT using electrical impedance tomography imaging," *Physiol. Meas.*, vol. 32, no. 1, p. 19, 2011.

[2] D. C. Barber and B. H. Brown, "Applied potential tomography," *J. Phys. E, Sci. Instrum.*, vol. 17, no. 9, p. 723, 1984.

[3] E. Lin and A. Alessio, "What are the basic concepts of temporal, contrast, and spatial resolution in cardiac CT?" *J. Cardiovascular Comput. Tomogr.*, vol. 3, no. 6, pp. 403–408, 2009.

[4] I. Frerichs *et al.*, "Chest electrical impedance tomography examination, data analysis, terminology, clinical use and recommendations: Consensus statement of the translational EIT development study group," *Thorax*, vol. 72, no. 1, pp. 83–93, 2017.

[5] A. Biguri, M. Dosanjh, S. Hancock, and M. Soleimani, "A general method for motion compensation in X-ray computed tomography," *Phys. Med. Biol.*, vol. 62, no. 16, p. 6532, 2015.

[6] T. Gupta and C. A. Narayan, "Image-guided radiation therapy: Physician's perspectives," *J. Med. Phys./Assoc. Med. Phys. India*, vol. 37, no. 4, pp. 174–182, 2012.

[7] D. Liu, V. Kolehmainen, S. Siltanen, A.-M. Laukkanen, and A. Seppänen, "Estimation of conductivity changes in a region of interest with electrical impedance tomography," *Inverse Problems Imag.*, vol. 9, no. 1, pp. 211–229, 2015.

[8] L. Miao, Y. Ma, and J. Wang, "ROI-based image reconstruction of electrical impedance tomography used to detect regional conductivity variation," *IEEE Trans. Instrum. Meas.*, vol. 63, no. 12, pp. 2903–2910, Dec. 2014.

[9] H. Kwon, A. L. McEwan, T. I. Oh, A. Farooq, E. J. Woo, and J. K. Seo, "A local region of interest imaging method for electrical impedance tomography with internal electrodes," *Comput. Math. Methods Med.*, vol. 2013, Jun. 2013, Art. no. 964918.

[10] M. Wang, Q. Wang, and B. Karki, "Arts of electrical impedance tomographic sensing," *Philos. Trans. Roy. Soc. A, Math., Phys., Eng. Sci.*, vol. 374, no. 2070, 2016, Art. no. 20150329.

[11] J. A. Victorino *et al.*, "Imbalances in regional lung ventilation: A validation study on electrical impedance tomography," *Amer. J. Respiratory Crit. Care Med.*, vol. 169, no. 7, pp. 791–800, 2004.

[12] S. Lindgren, H. Odenstedt, C. Olegård, S. Söndergaard, S. Lundin, and O. Stenqvist, "Regional lung derecruitment after endotracheal suction during volume-or pressure-controlled ventilation: A study using electric impedance tomography," *Intensive Care Med.*, vol. 33, no. 1, pp. 172–180, 2007.

[13] S. Leonhardt and B. Lachmann, "Electrical impedance tomography: The holy grail of ventilation and perfusion monitoring?" *Intensive Care Med.*, vol. 38, no. 12, pp. 1917–1929, 2012.

[14] T. I. Oh *et al.*, "Validation of a multi-frequency electrical impedance tomography (mfEIT) system KHU Mark1: Impedance spectroscopy and time-difference imaging," *Physiol. Meas.*, vol. 29, no. 3, pp. 295–307, 2008.

[15] C. L. Yang, T. T. Zhang, J. K. Seo, and M. Soleimani, "Localized frequency difference EIT for lung tumour monitoring," in *Proc. 15th Int. Conf. Biomed. Appl. Elect. Impedance Tomogr.*, 2014, p. 92.

[16] A. Borsic, B. M. Graham, A. Adler, and W. R. B. Lionheart, "Total variation regularization in electrical impedance tomography," School Math., Manchester Inst. Math. Sci., The Univ. Manchester, Manchester, U.K., Tech. Rep., 2007.

[17] Z. Zhou *et al.*, "Comparison of total variation algorithms for electrical impedance tomography," *Phys. Med. Biol.*, vol. 36, no. 6, p. 1193, 2015.

[18] H.-C. Kim, K. Y. Kim, J. W. Park, and H. J. Lee, "Electrical impedance tomography reconstruction algorithm using extended Kalman filter," in *Proc. ISIE*, Busan, South Korea, Jun. 2001, pp. 1677–1681.

[19] E. T. Chung, T. F. Chan, and X.-C. Tai, "Electrical impedance tomography using level set representation and total variational regularization," *J. Comput. Phys.*, vol. 205, no. 1, pp. 357–372, 2005.

[20] S. C. Chan, J. Kuen, J. Lee, E. J. Woo, D. Holder, and J. K. Seo, "Frequency-difference EIT (fdEIT) using weighted difference and equivalent homogeneous admittivity: Validation by simulation and tank experiment," *Physiol. Meas.*, vol. 30, no. 10, p. 1087, 2009.

[21] J. Jang and J. K. Seo, "Detection of admittivity anomaly on high-contrast heterogeneous backgrounds using frequency difference EIT," *Physiol. Meas.*, vol. 36, no. 6, pp. 1179–1192, 2015.

[22] J.-R. Wang, B.-Y. Sun, H.-X. Wang, S. Pang, X. Xu, and Q. Sun, "Experimental study of dielectric properties of human lung tissue *in vitro*," *J. Med. Biol. Eng.* vol. 34, no. 6, pp. 598–604, 2014.

[23] S. Grimnes and G. Martinsen, "Passive tissue electrical properties," in *Bioimpedance and Bioelectricity Basics*, 2nd ed. New York, NY, USA: Academic, 2008, ch. 4, pp. 93–137.

[24] J. Gao, S. Yue, J. Chen, and H. Wang, "Classification of normal and cancerous lung tissues by electrical impendence tomography," *Biomed. Mater. Eng.*, vol. 24, no. 6, pp. 2229–2241, 2014.

[25] A. Sujin, T. I. Oh, S. C. Jun, J. K. Seo, and E. J. Woo, "Validation of weighted frequency-difference EIT using a three-dimensional hemisphere model and phantom," *Physiol. Meas.*, vol. 32, no. 10, p. 1663, 2011.

[26] A. Sujin, T. I. Oh, S. C. Jun, J. Lee, J. K. Seo, and E. J. Woo, "Weighted frequency-difference EIT measurement of hemisphere phantom," *J. Phys., Conf. Ser.*, vol. 224, no. 1, 2010, Art. no. 012059.

[27] J. K. Seo, J. Lee, S. W. Kim, H. Zribi, and E. J. Woo, "Frequency-difference electrical impedance tomography (fdEIT): Algorithm development and feasibility study," *Physiol. Meas.*, vol. 29, no. 8, pp. 929–944, 2008.

[28] J. Wang, J. W. Ma, B. Han, and Q. Li, "Split Bregman iterative algorithm for sparse reconstruction of electrical impedance tomography," *Signal Process.*, vol. 92, no. 12, pp. 2952–2961, Dec. 2012.

[29] T. Goldstein and S. Osher, "The split Bregman method for L1-regularized problems," *SIAM J. Imag. Sci.*, vol. 2, no. 2, pp. 323–343, 2009.

[30] T. In *et al.*, "Calibration methods for a multi-channel multi-frequency EIT system," *Physiol. Meas.*, vol. 28, no. 10, p. 1175, 2007.

[31] A. Adler *et al.*, "GREIT: A unified approach to 2D linear EIT reconstruction of lung images," *Physiol. Meas.*, vol. 30, no. 6, pp. S35–S55, 2009.

Authors' photographs and biographies not available at the time of publication.